On-line Monitoring of Stator Inter-Turn Failures in DTC driven Asynchronous Motors using Mathematical Morphological Gradient

Hassan H. Eldeeb[1], Alberto Berzoy[2], Ahmed A. Saad[1], *Student Members*, *IEEE* and O.A. Mohammed[1], *Fellow, IEEE*

1- Energy System Research Laboratory, ECE Department, Florida International University, Miami, FL33174, USA

2- Sonnen Batterie Inc, Tucker, GA 30084, USA

helde002@fiu.edu

***Abstract*— This study presents an in-service non-intrusive diagnosis methodology for the detection of incipient faults in the induction motor's (IM) stator windings. The failure identification (FI) algorithm is based on the application of mathematical morphological gradient (MMG) technique on the stator's current in the time domain. The IM under study is driven by the direct torque control (DTC). Comprehensive investigation of harmonics, inter-harmonics and sub-harmonics content is conducted to compare between the FI based on the classical motor current signature analysis (MCSA), and the proposed technique. The proposed MMG based FI routine is fast, online, and easy to implement on digital controllers. The FI technique was validated through the co-simulation between the physics based finite element (FE) model of IM, and the voltage source inverter (VSI), DTC controller, and FI logic. The co-simulation have the merit of simulating the IM with all the harmonic content to improve the reliability of the FI. Moreover, it represents a trustworthy alternative to the experimental platform, which accelerate the ageing rate of the IM. Simulation reinforced by experimental results depicted the robustness of the FI method.**

Keywords*— Direct Torque Control, Diagnosis, Induction machine, Mathematical morphological gradient, FEA, Inter-Turn failures

I. Introduction

Inter-turn failure (ITF) in stator's windings is the second most frequent fault in induction motors (IM), after bearing faults [1]. The online detection of ITF at its embryonic stages is a vital key for the protection of the asynchronous motor drive system [2]. Consequently, online techniques of ITF fault identification (FI) are pervasive in literature.

The IM system could be categorized into three types: connected directly on-line (DOL), fed from open-loop controlled voltage source inverter (VSI), and fed from closed-loop VSI. The latter can be categorized on scalar and vector-controllers. The vector control algorithm employed in the majority of the high performance motor drive industries is the direct torque control (DTC), due to its robustness and could be implemented easily [3]. However, its robustness overburden the detection of ITFs at their initial stages, as the DTC controller hides the signatures present at the asymmetrical DOL connected IM.

Frequency spectrum investigation is widely used in online diagnosis of asynchronous motors stator's failures [4]. That investigation is commonly done for the stator's current ($\boldsymbol{i_s}$), and denoted as motor current signature analysis (MCSA). Monitoring the third order harmonic of $\boldsymbol{i_s}$, proved to be ineffective in detecting the incipient stator's fault, especially in the low voltage IMs, as supply unbalance or inherit IM asymmetries mimic the fault signatures, and could result in false FI [5]. Consequently, other harmonic orders were used to detect ITFs in DOL connected IM. In [6], three order harmonic components at $90, 120$ and 150 Hz were used to detect ITF in DOL fed IM, with supply frequency of 60 Hz. A model was developed in [7] for the induction motor (IM) with ITF to explore the interaction between the saturation in the asymmetrical machine and the spectral content of $\boldsymbol{i_s}$. ITF detection based on the radiated magnetic flux captured via an external magnetic loop for DOL connected IM was presented in [8]. The researchers claimed that FI based on the radiated flux is more accurate than MCSA, as the ITF creates its own current, and its own magneto-motive force. However, that claim was not supported by comparative analysis between both techniques.

Due to the fact that frequency domain transformations (FFT) are limited in their applications to stationary signals only, detection of ITF based on time-frequency domains gained popularity recently in literature. In [9]-[11] wavelet transformation (WT) was adopted to detect IM stator's fault. Whereas in [12], wavelet transformation was done over the radiated external magnetic flux from the IM for FI. The IM considered in the four aforementioned studies were DOL connected.

Stator's winding fault recognition is more vital in VSI fed IMs. The abrupt voltage transitions (dv/dt) accompanying high switching frequency (f_s) of the VSI intensifies the electric field stress over the insulations, which by its role accelerates the ITF propagation. Moreover, with the rapid growth in the electric vehicles industry [13], more attention should be given to FI of ITFs in vector controlled IMs, especially the DTC driven ones.

The first reaction of the DTC controller to the ITF is the increase in the 3rd order harmonic component of $\boldsymbol{i_s}$, to counter balance the oscillatory component in the developed torque [14]-

This work was partially supported by grants from the Office of Naval Research. The authors are with the Energy Systems Research Laboratory, Department of Electrical and Computer Engineering, Florida International University, Miami, FL 33174, USA (e-mail: mohammed@fiu.edu).

[15]. That's the reason why in [16] MCSA was used and the 3rd order harmonic component was adopted for FI. Whereas in [17], beside the MCSA, the authors used the increase in the positive sequence components (SC) of $\boldsymbol{i_s}$ in the synchronous rotating frame to counter-balance the negative SC due to ITF as FI. The latter technique was implemented on DSP controller in [18]. As the ITF will introduce a 2nd order harmonic component in the developed torque [15], the developed power will inherit the same signature. Consequently in [19], the FI was based on monitoring of the 2nd order harmonic component of the developed power, for DOL connected IM and DTC driven IM. The signatures were much more obvious in the DOL connected IM than the DTC driven one, due to the compensatory nature of the DTC controller. Finally, the FI or ITFs in DTC driven IMs based on the off-diagonal components of the symmetrical components impedance matrix was presented in [20]. The FI routine has the advantages of being in time domain, and immune against sensor errors and motor inherited asymmetries. However, the fundamental frequency got affected by the stator's fault, hence a robust frequency estimation technique is required in that FI routine.

From the aforementioned literature survey, it is obvious that the 5 researches have investigated FI of ITFs in DTC driven IMs were either in frequency domain completely, or require frequency estimator for the transformation. None of the aforementioned researches dealt with the signal directly in the time domain (T-domain). Among the various T-domain signal processing routines, mathematical morphological gradient (MMG) theory, that was initiated for image processing applications [21], showed promising results in detecting broken bar faults [22], and ITFs [23] for DOL connected IMs.

The contribution of this study to the current state-of-the-art is the development of a non-intrusive, non-destructive online FI technique based on MMG filters applied on $\boldsymbol{i_s}$ for DTC driven asynchronous motors. Moreover, physics based co-simulation is presented for FI in DTC controlled IM, through the coupling between: finite element analysis (FEA) of IM and VSI and DTC models. Simulation and experimental results demonstrating the FI technique is able to detect ITSC faults. Furthermore, comparative analysis is given between the proposed FI and the MCSA based FI.

II. Overview of DTC

The co-simulation platform and the FI routine of the DTC driven asynchronous motor under study is shown in Fig.1. The DTC algorithm is based on two hysteresis controllers , the first is a two-level one to control the developed torque (T_e), while the other is a three-level one used to control the magnitude of the flux-linkage ($|\boldsymbol{\lambda_s}|$). In this article the DTC controller is implemented with a fixed switching frequency ($f_s = 10$ kHz). It's noteworthy to mention that T_e and $|\boldsymbol{\lambda_s}|$ are not measured by the DTC controllers, they are estimated. The DTC algorithm procedure could summarized in the following 7 steps:

1) Measurement of VSI signals'

The first step is the measurement of the DC-link voltage (V_{DC}) and the motor's line current($\boldsymbol{i_s}$).

2) Transformation into $\alpha\beta$ coordinates

The measured values are transformed from the three-phase stationary frame of reference abc into the two-phase stationary frame of reference $\alpha\beta$ via Clark's transformation.

3) Stator's voltage estimation

The space-vector (SV) output voltage of the VSI ($\boldsymbol{\hat{v}_s}$) could be estimated through the knowledge of V_{DC} and the switching sequence ($[\boldsymbol{d_i}] = [d_{ia} \quad d_{ib} \quad d_{ic}]^t$).

4) Estimation of T_e and $\boldsymbol{\lambda_s}$

Using $\boldsymbol{\hat{v}_s}$ and $\boldsymbol{i_s}$, the developed torque and the flux-linkage could be estimated by (1) and (2), respectively. R_s is the stator resistance.

$$\hat{T}_e = \frac{3}{2}\frac{P}{2}\frac{L_m}{L_s}\left(i_{s\beta}\hat{\lambda}_{s\alpha} - i_{s\alpha}\hat{\lambda}_{s\beta}\right) \quad (1)$$

$$\boldsymbol{\hat{\lambda}_s} = \int(\boldsymbol{v_s} - R_s\boldsymbol{i_s})dt \quad (2)$$

5) Controllers action

The error between the estimated and reference values of T_e and $\boldsymbol{\lambda_s}$ are the inputs for the aforementioned hysteresis controllers. $\delta|\boldsymbol{\lambda_s}| = \lambda_{ref} - |\boldsymbol{\lambda_s}|$ and $\delta T_e = T_{ref} - T_e$ are the errors in $\boldsymbol{\lambda_s}$ and T_e, respectively. The output of the hysteresis controller are the (ψ, τ signals) indicate to the switching table (Look-up Table) the requirements, as in Fig. 2.

6) Sector detection

Based on τ and ψ, the sector (S_x, where$x = \{1-6\}$) where the flux-linkage lies is determined.

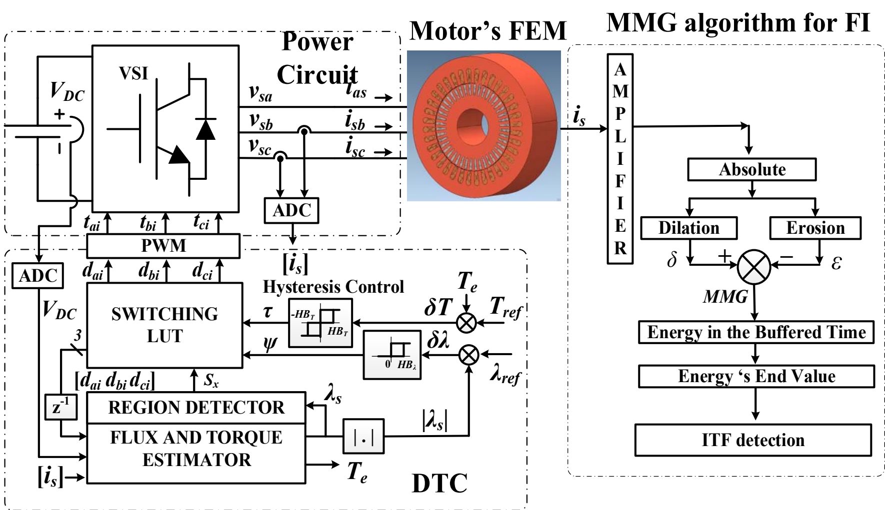

Fig. 1. Co-simulation platform for DTC driven faulty IM system study and FI routine

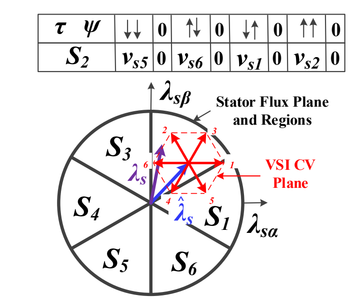

Fig. 2. Estimated and actual Stator Flux $\boldsymbol{\lambda_s}(t_k)$

TABLE I. Switching Look-up Table For Classical DTC

τ, ψ	↓↓	0	↑↓	0	↓↑	0	↑↑	0
S_1	$\boldsymbol{v_{s4}}$	0	$\boldsymbol{v_{s2}}$	0	$\boldsymbol{v_{s5}}$	0	$\boldsymbol{v_{s3}}$	0
S_2	$\boldsymbol{v_{s5}}$	0	$\boldsymbol{v_{s6}}$	0	$\boldsymbol{v_{s1}}$	0	$\boldsymbol{v_{s2}}$	0
S_3	$\boldsymbol{v_{s1}}$	0	$\boldsymbol{v_{s4}}$	0	$\boldsymbol{v_{s3}}$	0	$\boldsymbol{v_{s6}}$	0
S_4	$\boldsymbol{v_{s3}}$	0	$\boldsymbol{v_{s5}}$	0	$\boldsymbol{v_{s2}}$	0	$\boldsymbol{v_{s4}}$	0
S_5	$\boldsymbol{v_{s2}}$	0	$\boldsymbol{v_{s1}}$	0	$\boldsymbol{v_{s6}}$	0	$\boldsymbol{v_{s5}}$	0
S_6	$\boldsymbol{v_{s6}}$	0	$\boldsymbol{v_{s3}}$	0	$\boldsymbol{v_{s4}}$	0	$\boldsymbol{v_{s1}}$	0

7) VSI switching signals

Via the detected sector S_x, and the controllers output signals (ψ, τ), the output switching signals to the gates of the VSI switches are determined based on the DTC look-up table, shown in Table I.

III. MCSA: ITF effect and DTC reaction Through Harmonic Insertion

ITF results in escalating the positive SC, and insertion of negative SC in $\boldsymbol{i_s}$ [14]-[15]. Thereby, $\boldsymbol{i_s}$ will be as in (3):

$$\boldsymbol{i_s} = |\bar{I}_{sP}| e^{j\left(\omega t + \phi_{i_{sP}}\right)} + |\bar{I}_{sN}| e^{-j\left(\omega t + \phi_{i_{sN}}\right)} \tag{3}$$

where $|\bar{I}_{sP}|$ and $|\bar{I}_{sN}|$ are the magnitudes of the positive and negative SC of i_s, respectively, $\omega = 2\pi f$. It's noteworthy to mention that those SCs are observable by the DTC via the current transducers.

Based on (2), $\hat{\lambda}_s$ will inherit a negative SC, and will suffer of suppression in the positive SC. $\hat{\lambda}_s$ in the space-vector notation will be as in (4):

$$\hat{\lambda}_s = \left|\bar{\lambda}_{sP}\right| e^{j\left(\omega t + \phi_{\lambda_{sP}}\right)} + \left|\bar{\lambda}_{sN}\right| e^{-j\left(\omega t + \phi_{\lambda_{sN}}\right)} \tag{4}$$

where $\left|\bar{\lambda}_{sP}\right|$ and $\left|\bar{\lambda}_{sN}\right|$ are the magnitudes of the positive and negative SC of $\hat{\lambda}_{s,}$ respectively. But T_e could be written as in (5) instead of (1):

$$\hat{T}_e = \frac{3}{2}\frac{p}{2}\frac{L_m}{L_s}\mathrm{Im}\{\boldsymbol{\hat{\lambda}_s}^{*}\boldsymbol{i_s}\} \tag{5}$$

Consequently, from (3) and (4) in (5), $\hat{T}_e$ will have two terms in summation, as in (6): the first is constant (observable static error), while the second represents the oscillatory component at $2\omega_e$ (observable dynamic error).

$$\hat{T}_e = \frac{3}{2}\frac{P}{2}\frac{L_m}{L_s}\left(T_{\text{stat\_obs}} + \left|\bar{T}_{\text{dyn\_obs}}\right| \sin(2\omega_e t + \gamma)\right) \tag{6}$$

DTC tends to compensate the observable error through introducing a $3f$ component in $\boldsymbol{i_s}$ (and hence in $\boldsymbol{\hat{\lambda}_s}$). The aforementioned 3rd order harmonic will counterbalance the oscillatory torque error observed by the torque controller.

Stator's fault introduces inter-harmonics in the stator's current at frequencies (f_{ITSC}) [19], as in (7):

$$f_{ITSC} = f[\frac{m}{p}(1-s) \pm l] \tag{7}$$

where, $m = 0,1,2 \ldots$, $l = 0,1,3,5 \ldots$.

The interaction between the TIF, and the saturation in the stator as its result, produces third-order-related inter-harmonic components as in (8) [7].

$$f_{3h} = f[\frac{R}{p}(1-s) \pm 3] \tag{8}$$

where R is the number of rotor's slots.

Various other harmonics/inter-harmonic components appears in the stator's current, even for healthy IMs, as a result of the rotor slot effects, its interaction with saturation, switching activity of VSI, etc. Those harmonic components and their causes are explained in details in [15], and could be summarized as in Table II. It was proven experimentally in [15], the difficulty of FI based on MCSA due to the numerous harmonics/inter-harmonics existence.

TABLE II. Summary of predicted Harmonics DTC driven faulty IM.

Cause	Generated harmonics in stator's Current	
Rotor slots effect	$f_{LF\_RHS} = f\left[1 - \frac{R\beta}{p}(1-s)\right]$	(9)
	$f_{HF\_RHS} = f\left[1 + \frac{R\beta}{p}(1-s)\right]$	(10)
Saturation effect	$f_{RSH\_sat} = f\left[1 \pm 2\alpha \pm \frac{R}{p}(1-s)\right]$	(11)
ITSC effect	$f_{ITSC} = f\left[\frac{m}{p}(1-s) \pm l\right]$	(7)
ITSC and Saturation effect	$f_{3h} = f\left[\frac{R}{p}(1-s) \pm 3\right]$	(8)
DTC reaction	$f_{DTC\_reaction} = 3f$	(12)

IV. Mathematical Morphological Gradient Algorithm for FI

Mathematical morphology (MM) can be defined as a technique for the analysis of spatial structures, based on set theory, integral geometry and lattice algebra [21]. The main application of the MM is the image and video processing. It is totally different from the methods that are based on integral transform, such as Fourier Transform (FT) and Wavelet Transform (WT), in basic principles, algorithmic operations and approach. In contrast to the theory of linear signal processing, such as FT/WT, MM is non-linear signal processing technique [25]. Furthermore, it depends on the shape of a signal waveform in the time domain rather than the frequency domain.

The main purpose of morphological operators is to extract related structures of a set. The extraction is performed by interaction between the set of the signal data and another probing set, which is called Structuring Element (SE). The shape of the SE is pre-defined according to some priori information about the morphological form of the signal.

There are two basic morphological operators, dilation and erosion, which form a pair of dual transforms. The logic behind the mathematical morphological gradient (MMG) theory is to recognize the pattern in a non-linear signal in the time domain by adapting it through the interaction with the MMG operator. This interaction is done via the basic logical operators of MMG: dilation (δ) and erosion (ε). Let m denote a signal and g denote a SE, and the length of g be noticeably shorter than that of m. The signal is defined as a single dimension gray-scale image and it is proceeded by dilation operation as in (13):

$$\delta = (m \oplus g) = max\ \left\{m(x+s) + g(s) | (x+s) \in D_m, s \in D_g\right\} \tag{13}$$

where $\oplus$ dilation operator means m dilated with g to produce the dilated signal δ. Whereas D_m, D_g are the definition domain of m and g respectively, and x is the samples of signal m. In the case under study, the signal m is the stator's current $\boldsymbol{i_s}$.

Erosion can be described as shrinking of the shapes contained in the input signal by using the SE [21]. Erosion is labelled the same equation but instead of supreme will be replaced by minutest as in (14),

$$\varepsilon = (m \ominus g) = min\left\{m(x+s) + g(s) | (x+s) \in D_m, s \in D_g\right\} \tag{14}$$

where $\ominus$ erosion operator means m eroded with g, and ε is the eroded signal.

MMG is defined as the arithmetic difference between the dilation and erosion of a signal by the SE. The MMG aims at removing the steady state components and highlights the transient's ones. The MMG is represented as in (15),

$$MMG = \delta - \varepsilon \tag{15}$$

Meanwhile dilation and erosion using a flat SE return the maximum and minimum of the signal samples, for each point, its morphological gradient reflects the change between maximum and minimum obtained within the samples of the SE.

V. Co-Simulation Results

A 1 HP WEG IM of M19 USS iron cored stator with 36 slots is used in this study. The rotor has 44slots, and aluminum bars of 3.8×10^7℧/m. The IM has an air gap of 0.31 mm. Each phase total number of turns per phase is $N_{as} = 510$. Four taps were done on the physical IM and the FEA model to study the ITF. The fault severity factor (μ_f) is a ratio between the number of turns short-circuited and N_{sa}.The four faulty cases ($C_1 - C_4$) are for $\mu_f = 1.08\%, 2.68\%, 3.98\%$ and 4.7%, respectively. The fault resistance $R_f = 0.67\ \Omega$. The nameplate ratings and parameters of the IM are shown in Table III. Co-simulation environment was realized via the interactive coupling between the DTC-VSI models in *Simulink/MatLab* environment and the FEA model of IM in *MagNET/Infolytica*. For both experimental and Co-simulation test, the torque reference value was $T_{ref} = 2$ Nm.

A. FI based on MMG

TABLE III. Nameplate ratings of the 1 Hp WEG IM under study.

Param.	Value	Param.	Value	Rating	Value	Rating	Value
L_{ls} (mH)	32.1	$R_s(\Omega)$	9.292	P_r (W)	746	PF	0.8
L_{lr}(mH)	37.0	$R_r(\Omega)$	7.231	V_r(V)	460	*poles*	4
L_m(H)	0.895	$J_m(Kgm^2)$	0.053	I_r (A)	1.47	n_r (rpm)	1730

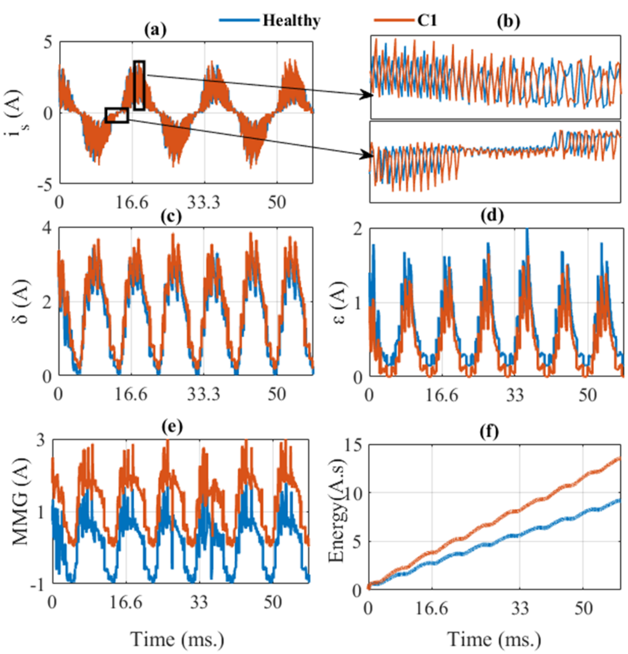

Fig. 3. FEA Co-Simulation results for healthy and C1 faulty case (a): $\boldsymbol{i_s}$ in T-domain, (b): Zoom-in of $\boldsymbol{i_s}$ at zero-crossing at at the peak, (c): Dilataed signal, (d): Eroded Signal, (e): MMG, (f): Accumulated energy.

The stator's current was obtained for healthy and C_1 faulty conditions from the FEA co-simulation environment, as shown in Fig. 3(a). Zooming of $\boldsymbol{i_s}$ of both are shown in Fig.3(b). The dilation and erosion of the obtained signals are displayed in Fig. 3(c) and Fig. 3(d), respectively. As Fig. 3(c) shows, the maximums of the faulty cases are larger than those for the healthy case. Whereas in Fig. 3(d), the eroded signal has higher value in the healthy case if compared to C_1. Thereby, MMG, has higher value in C_1 case if compared to the healthy, as in Fig. 3(e). To discriminate the ITFs, the area under the curves of Fig. 3(e) are calculated and denoted as 'Energy', as in Fig. 3(f). The ITFs detection is based on the end value of the energy at the processing window. That energy end value was 9.185 A. s and 13.5 A. s for healthy and C_1 cases, respectively

B. FI based on MCSA

To compare with the MCSA based FI algorithms, the harmonic spectrum of $\boldsymbol{i_s}$ was obtained, up to the 8th order harmonic ($h = \text{frequency(Hz)}/f$), by FFT with sampling frequency of 20 kHz. Results showed that numerous sub-harmonics, inter-harmonics and harmonics are present in case of healthy and faulty IM driven by DTC controller, due to the reasons mentioned in section III. Those harmonics are not always greater in amplitude in case of faulty IM. As expected, the fault will amplify the 3rd order harmonic component if the current, due to the DTC reaction. However, that 3rd order content was present in case of healthy motor, due to inherent asymmetries in the motor design, which makes the FI through monitoring that component problematic.

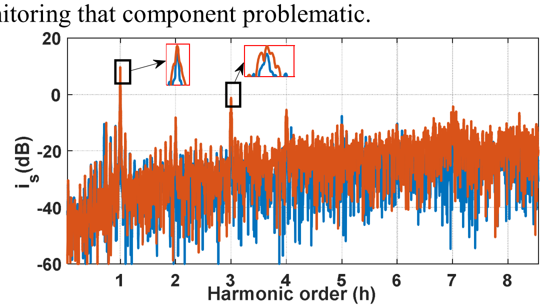

Fig. 4. Frequency spectrum of $\boldsymbol{i_s}$ in Co-simulation enviroment

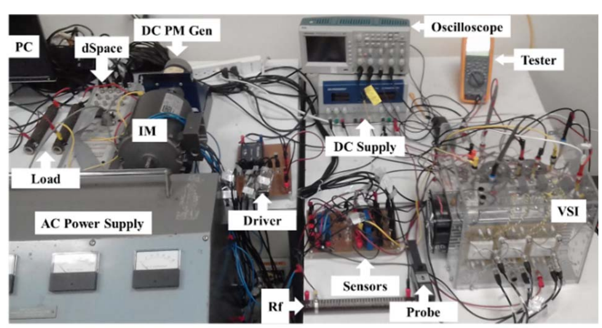

Fig. 5. Experimental setup for acquisition with a dSpace 1104.

VI. Experimental Results

The experimental test platform is shown in Fig. 5. The 1 HP IM's shaft is mechanically coupled to a 250 W and 42 V dc permanent magnet (PM) machine. The dc PM machine is acting as a generator with variable load. A dSpace 1104 board is used for the control and condition monitoring. The motor angular speed is measured with a 1000 ppr coupled to the PM machine. The healthy condition as well as the 4 faulty conditions were run experimentally in the setup, and MMG FI routine, as well as FFT were performed to the stator current.

A. FI based on MMG

The MMG routine is applied on $\boldsymbol{i_s}$, and the energy's end values (EEV) are displayed in Table IV. For better judgement on the proposed CM technique, the EEV of the healthy cases were taken a reference, and the EEVs were calculated as percentage with respect to it, according to (16):

$$EEV\ (\%) = \left(\frac{EEV_{faulty} - EEV_{healthy}}{EEV_{healthy}}\right) \times 100 \qquad (16)$$

TABLE IV. MMG EXPERIMENTAL RESULTS

N_{sa2}	μ_f (%)	Cases	EEV	EEV(%)
0	0	healthy	9.18	0
6	1.08	C1	12	30.72
14	2.68	C2	13.4	45.9
20	3.98	C3	15.4	67.76
24	4.70	C4	16.4	78.6

As Table IV depicts, the proposed MMG technique was able to detect embryonic faults experimentally. Even for the 1.08% fault, the EEV as percentage was 30.7%, which is very significant to notice that small ITF.

B. Comparative analysis between the proposed MMG based FI and MCSA based FI

To investigate the effectiveness of the proposed technique, comparative analysis was done in the experimental platform between the proposed MMG based FI and the convetional MCSA based FI for the DTC driven IM with ITFs. The setup was run experimentally under the five conditions, and the spectrum of $\boldsymbol{i_s}$ is displayed in Fig.6. From Fig. 7 it is obvious that none of the harmonic orders classically used for CM (fundamental, 3rd, 5th, 6th and 7th orders) was able detect and discriminate the faults in order of μ_f. Per instance, the healthy has higher fundamental component than $C_1$and C_2, but less than C_4. Whereas at the 3rd order harmonic, all the faulty cases have higher value from the healthy one, but the difference between the faulty ones is not significant. Moreover, at the 6th and 7th order harmonics, the healthy case coincide with C_1, and it is hard to discriminate between them. Another interesting point is to notice that the experimental results matched with the co-simulation

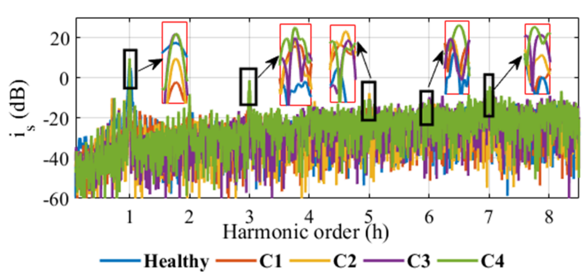

Fig. 6. Expiremental result: Spectrum of *C4* faulty IM's current at T_{ref_2}

results, which makes the co-simulation platform convenient alternative to avoid subjecting the machine to short-circuit that might accelerate its ageing process.

VII. Conclusion

A novel MMG based FI technique was proposed to detect stator inter-turn failures in DTC driven asynchronous motors was presented in this study. Co-simulation results reinforced by the experimental results showed the capability of the proposed non-intrusive non-destructive online FI technique to detect the TIF faults in time-domain more accurately than the conventional MCSA. Among the advantages of the proposed technique is: unlike the MCSA based FI, which requires monitoring of several harmonics/inter-harmonics to detect the fault, Mat-Morph CM is based on monitoring one value. In addition, Mat-Morph routine in its basic concept is based on buffering, addition and subtraction, which make it easy to implement on digital signal processing boards.

VIII. References

[1] X. Liang and K. Edomwandekhoe, "Condition monitoring techniques for induction motors," 2017 IEEE Industry Applications Society Annual Meeting, Cincinnati, OH, 2017, pp. 1-10

[2] M. Riera-Guasp, J. A. Antonino-Daviu and G. A. Capolino, "Advances in Electrical Machine, Power Electronic, and Drive Condition Monitoring and Fault Detection: State of the Art," in IEEE Transactions on Industrial Electronics, vol. 62, no. 3, pp. 1746-1759, March 2015

[3] S. Cheng, P. Zhang and T. G. Habetler, "An Impedance Identification Approach to Sensitive Detection and Location of Stator Turn-to-Turn Faults in a Closed-Loop Multiple-Motor Drive," in IEEE Transactions on Industrial Electronics, vol. 58, no. 5, pp. 1545-1554, May 2011

[4] G. A. Capolino, J. A. Antonino-Daviu and M. Riera-Guasp, "Modern Diagnostics Techniques for Electrical Machines, Power Electronics, and Drives," in IEEE Transactions on Industrial Electronics, vol. 62, no. 3, pp. 1738-1745, March 2015

[5] S. M. A. Cruz and A. J. M. Cardoso, "Diagnosis of stator inter-turn short circuits in DTC induction motor drives," IEEE Trans. Ind. Appl., vol. 40, no. 5, pp. 1349–1360, Sep. 2004.

[6] S. E. Pandarakone, Y. Mizuno and H. Nakamura, "Frequency spectrum investigation and analytical diagnosis method for turn-to-turn short-circuit insulation failure in stator winding of low voltage induction motor," in IEEE Transactions on Dielectrics and Electrical Insulation, vol. 23, no. 6, pp. 3249-3255, Dec. 2016

[7] S. Nandi, "A detailed model of induction machines with saturation extendable for fault analysis," in IEEE Transactions on Industry Applications, vol. 40, no. 5, pp. 1302-1309, Sept.-Oct. 2004.

[8] M. Irhoumah, R. Pusca, E. Lefevre, D. Mercier, R. Romary and C. Demian, "Information Fusion With Belief Functions for Detection of Interturn Short-Circuit Faults in Electrical Machines Using External Flux Sensors," in IEEE Transactions on Industrial Electronics, vol. 65, no. 3, pp. 2642-2652, March 2018.

[9] N. R. Devi, D. V. S. S. Siva Sarma and P. V. Ramana Rao, "Diagnosis and classification of stator winding insulation faults on a three-phase induction motor using wavelet and MNN," in IEEE Transactions on Dielectrics and Electrical Insulation, vol. 23, no. 5, pp. 2543-2555, October 2016.

[10] N. Rama Devi, D. V. S. S. Siva Sarma and P. V. Ramana Rao, "Detection of stator incipient faults and identification of faulty phase in three-phase induction motor – simulation and experimental verification," in IET Electric Power Applications, vol. 9, no. 8, pp. 540-548, 9 2015.

[11] R. Kechida, A. Menacer, H. Talhaoui and H. Cherif, "Discrete wavelet transform for stator fault detection in induction motors," 2015 IEEE 10th International Symposium on Diagnostics for Electrical Machines, Power Electronics and Drives (SDEMPED), Guarda, 2015, pp. 104-109.

[12] H. Cherif, A. Menacer, R. Romary and R. Pusca, "Dispersion field analysis using discrete wavelet transform for inter-turn stator fault detection in induction motors," 2017 IEEE 11th International Symposium

on Diagnostics for Electrical Machines, Power Electronics and Drives (SDEMPED), Tinos, 2017, pp. 104-109.
[13] Hassan H. Eldeeb, Samy Faddel, Osama A. Mohammed, "Multi-Objective Optimization Technique for the Operation of Grid tied PV Powered EV Charging Station", Electric Power Systems Research, Volume 164, pp. 201-211, Nov. 2018.
[14] A. Berzoy, O. A. Mohammed and J. Restrepo, "Analysis of the Impact of Stator Interturn Short-Circuit Faults on Induction Machines Driven by Direct Torque Control," in IEEE Transactions on Energy Conversion, vol. 33, no. 3, pp. 1463-1474, Sept. 2018.
[15] H. H. Eldeeb, A. Berzoy and O. Mohammed, "Comprehensive Investigation of Harmonic Signatures Resulting from Inter- Tum Short-Circuit Faults in DTC Driven IM Operating in Harsh Environments," 2018 XIII International Conference on Electrical Machines (ICEM), Alexandroupoli, Greece, 2018, pp. 2579-2585
[16] S. S. Refaat, H. Abu-Rub, and A. Iqbal, "ANN-based system for inter-turn stator winding fault tolerant DTC for induction motor drives," in 2015 17th European Conference on Power Electronics and Applications (EPE'15 ECCE-Europe), 2015, pp. 1–7.
[17] S. M. A. Cruz and A. J. M. Cardoso, "Diagnosis of stator inter-turn short circuits in DTC induction motor drives," IEEE Trans. Ind. Appl., vol. 40, no. 5, pp. 1349–1360, Sep. 2004.
[18] S. M. A. Cruz, H. A. Toliyat, and A. J. M. Cardoso, "DSP implementation of the multiple reference frames theory for the diagnosis of stator faults in a DTC induction motor drive," IEEE Trans. Energy Convers., vol. 20, no. 2, pp. 329–335, Jun. 2005.
[19] M. Drif and A. J. M. Cardoso, "Stator Fault Diagnostics in Squirrel Cage Three-Phase Induction Motor Drives Using the Instantaneous Active and Reactive Power Signature Analyses," in IEEE Transactions on Industrial Informatics, vol. 10, no. 2, pp. 1348-1360, May 2014.
[20] A. Berzoy, H. H. Eldeeb and O. Mohammed, "Online fault detection of stator winding faults in IM driven by DTC using the off-diagonal term of the symmetrical component impedance matrix," 2018 IEEE Applied Power Electronics Conference and Exposition (APEC), San Antonio, TX, 2018, pp. 2482-2487.
[21] J. Serra and Ph. Salembier (Eds.), "Mathematical Morphology and its Application to Signal Processing", Int'l. Workshop on Mathematical Morphology and its Applications to Signal Processing (ISMM), 1993.
[22] J. de Jesus Rangel-Magdaleno, H. Peregrina-Barreto, J. M. Ramirez-Cortes, P. Gomez-Gil and R. Morales-Caporal, "FPGA-Based Broken Bars Detection on Induction Motors Under Different Load Using Motor Current Signature Analysis and Mathematical Morphology," in IEEE Transactions on Instrumentation and Measurement, vol. 63, no. 5, pp. 1032-1040, May 2014
[23] Y. Zhang, T. Y. Ji, M. S. Li and Q. H. Wu, "Application of morphological max-lifting scheme for identification of induction motor stator inter-turn short circuit," in CSEE Journal of Power and Energy Systems, vol. 1, no. 4, pp. 92-100, Dec. 2015
[24] I. Takahashi and T. Noguchi, "A New Quick-Response and High-Efficiency Control Strategy of an Induction Motor," in IEEE Transactions on Industry Applications, vol. IA-22, no. 5, pp. 820-827, Sept. 1986.
[25] A. Baug, N. R. Choudhury, R. Ghosh, S. Dalai and B. Chatterjee, "Identification of single and multiple partial discharge sources by optical method using mathematical morphology aided sparse representation classifier," in IEEE Transactions on Dielectrics and Electrical Insulation, vol. 24, no. 6, pp. 3703-3712, Dec. 2017.

.